LRP 508/94 October 1994

ALFVEN WAVE HEATING AND STABILITY

L. Villard, S. Brunner, A. Jaun and J. Vaclavik

Preprint of an Invited talk given at the
International Workshop on Alfvén Waves
in Honor of Prof. Hannes Alfvén,
Rio de Janeiro, Brazil,
8-10 November, 1994

Alfvén Wave Heating and Stability

L.Villard, S.Brunner, A.Jaun and J. Vaclavik

Centre de Recherches en Physique des Plasmas
Association Euratom - Confédération Suisse
Ecole Polytechnique Fédérale de Lausanne
21, av. des Bains – CH-1007 Lausanne/Switzerland

Abstract

Alfvén waves in fusion plasmas play an important role in a number of situations. First, in Alfvén Wave Heating (AWH) schemes. Second, both theory and experiment have demonstrated the existence of Global Alfvén Eigenmodes (GAEs). GAEs have been observed in different tokamaks (PRETEXT, TCA, TEXTOR, etc.) and, more recently, in a stellarator (Wendelstein 7-AS) where they were shown to become unstable under intense Neutral Beam injection. Third, the existence and possible destabilization by fast ions of Toroidicity induced Alfvén Eigenmodes (TAEs) has been evidenced both theoretically and experimentally. This destabilization could hamper the operation of a magnetically confined fusion reactor by setting a limit on the number of fusion alpha particles in the plasma. It is therefore crucial to understand the mechanisms leading to the occurence of the instability and also those that can stabilize the TAEs by increasing the strength of the damping. The aim is to be able to devise possible ways to avoid the instability of Alfvén eigenmodes in a region of parameter space that is compatible with the functionning of a fusion reactor. A global perturbative approach is presented to tackle the problem of the linear stability of TAEs. Our model computes the overall wave particle power transfers to the different species and thus could also be applied to the study of alpha power extraction in the presence of Alfvén waves. We indicate also how to go beyond the perturbative approach.

1 Introduction

This paper focuses on some aspects of Alfvén waves in laboratory fusion plasmas of the tokamak type. Several attempts have been made to heat the plasma in the Alfvén range of frequencies [1]-[4] and also to drive the plasma current non-inductively [5] . More recently, it has been shown theoretically [6]-[10] and in TFTR [11] and DIII-D [12], [13] experiments that some Alfvén eigenmodes (the TAEs) can become unstable in the presence of fast ions. Such fast ions can arise under intense Neutral Beam Injection (NBI) or in Ion-Cyclotron heated plasmas in the minority regime that creates a high energy tail in the ion velocity distribution. In a reactor plasma a population of energetic alpha particles will develop. It is important to predict whether the Alfvén instability hampers the operation of the machine.

The theory of Alfvén wave propagation, absorption and destabilization dates from several decades. A complete review of the theory of Alfvén wave heating is given in Ref.[14]. The first theoretical work on the destabilization of Alfvén waves by fast ions is reported in Ref. [15]. Since the discovery of the toroidicity induced Alfvén eigenmode (TAE) [16] much work has been devoted to this subject [6]-[13], [17]-[19]. The purpose of this paper is not to make a review of all these works but to highlight some of the main points in this context and to present recent developments in the understanding of Alfvén instabilities: a global approach, in which kinetic effects are considered as a perturbation of the ideal modes, will be presented and some results will be discussed.

The paper is structured as follows. In the next section, we present a brief overview of the spectrum of Alfvén waves as predicted from various physical models in 1-D and 2-D geometries. The damping and instability drive mechanisms are presented in Section 3. In Section 4 we introduce three different models in toroidal geometry. Some typical results of these models are shown in Section 5, which treats the cases of antenna excitation of Alfvén waves, and in Section 6, which analyzes their stability in the presence of fast ions.

2 Spectrum of Alfvén waves

In a cold, magnetized, current-carrying, cylindrical plasma column, neglecting electron inertia [20] the spectrum of Alfvén waves contains global Alfvén eigenmodes (GAEs) [21] and a continuum. The GAE wavefields have a global structure and their eigenfrequencies lie just below the corresponding continua. The GAEs belong to the same branch as the current-driven external kink instabilities. For large parallel wave numbers their frequency lie just below the ion cyclotron frequency [20] and the GAEs can be identified with the ion cyclotron waves. The Alfvén continuum eigenmodes are singular at the spatial Alfvén

resonances which, in a single ion species plasma, are defined by

$$\omega = \frac{v_A k_\parallel}{\sqrt{1 + \frac{v_A^2 k_\parallel^2}{\omega_{ci}^2}}} \tag{1}$$

In a cylinder modelling a tokamak of major radius R_0 the parallel wave number $k_\parallel$ can be written as

$$k_\parallel = \frac{1}{R_0}(n + \frac{m}{q}) \tag{2}$$

where n is the toroidal mode number, m is the poloidal mode number and q is the safety factor. Let us define a local magnetic set of orthornormal unit vectors which will be used throughout the paper: $\vec{e}_n = \nabla\psi/|\nabla\psi|$, $\vec{e}_\parallel = \vec{B}_0/B_0$, $\vec{e}_b = \vec{e}_\parallel \times \vec{e}_n$, where ψ is the poloidal flux function and B_0 is the equilibrium magnetic field. It can be shown that the wavefield components E_n and B_b have a singularity behaviour as $1/(\psi - \psi_{res})$ where ψ_{res} is the radial position of the shear Alfvén resonance defined by Eq.(1). The components E_b, B_n and $B_\parallel$ have a logarithmic type of singularity. The singularity is resolved by adding a small imaginary part in the dielectric tensor: ω is replaced by $\omega(1+i\nu)$, with $\nu > 0$ to ensure causality. The limit $\nu \to 0$ gives a finite power absorption. In the frame of the cold plasma and ideal MHD models, this absorption, called resonance absorption or continuum damping, is the only absorption mechanism. Also present in the spectrum of the cold plasma model are the radial eigenmodes of the fast magnetosonic wave, sometimes called 'compressional Alfvén wave'. It includes the surface mode which is the first radial eigenmode of the fast wave for $m = -1$. The surface mode eigenfrequency, in a plasma with a density profile, lies in the shear Alfvén continuum and its presence enhances the coupling from an antenna placed in the vacuum region. This property was used in the Alfvén wave heating experiments conducted in the TCA tokamak [2]: the idea is to excite the surface mode and to deposit the wave energy near the shear Alfvén resonance. The names 'compressional' and 'shear' qualifying the Alfvén waves should not be considered too strictly, in the sense that in inhomogeneous plasmas the 'shear' Alfvén waves have a small but finite compressibility (finite $B_\parallel$). This point will be illustrated further in the paper. The finite $B_\parallel$ of GAEs implies that these modes can be excited by an antenna: the radial component of the Poynting vector, $E_b B_\parallel$, is finite.

When finite Larmor radius (FLR) effects are taken into account (hot plasma model) there is no Alfvén continuum but instead a discrete set of damped eigenmodes of the kinetic Alfvén wave (KAW). The first radial eigenmode is usually the most weakly damped and subsists in the cold plasma limit. It is therefore identified as a GAE. If electron inertia is included in the model, the spectrum contains also eigenmodes of the surface quasi-electrostatic wave (SQEW) [14]. The electron and ion Landau dampings, the transit time magnetic pumping (TTMP) damping and the ion cyclotron damping are included

in the hot plasma model. There is no resonance absorption in this model; instead, mode conversion occurs to either the KAW (if $v_A/v_{te} < 1$) or the SQEW (if $v_A/v_{te} > 1$). The KAW propagates inwards and the SQEW propagates outwards from the mode conversion surface. The cold and hot plasma models are related by the following: when the mode converted waves are damped before reaching the plasma centre (KAW) or edge (SQEW) the total powers absorbed given by both models are the same. If that is not the case, the mode converted wave can establish a standing wave and a peak appears in the plasma response [22] that has no equivalent in the cold plasma model.

In toroidal axisymmetric geometry the finite aspect ratio couples the poloidal wave numbers m to each other; m is therefore not a good quantum number. In the cold plasma model the spatial Alfvén resonance condition of Eq.(1) is expressed by a differential equation involving the operator $\nabla_{||}$ to be solved on a magnetic surface ($\psi = const$). Therefore shear Alfvén resonances coincide with magnetic surfaces. When a cyclotron frequency surface $\omega = \omega_{ci}$ is present in the discharge, all magnetic surfaces intersecting the cyclotron surface are singular, thereby forming a 2-D continuum [23]. The toroidicity implies that in AWH scenarios there are usually several resonance surfaces, each of them absorbing a fraction of the total power. This makes power deposition in the centre of the discharge difficult, even more so in small aspect ratio, elongated or shaped plasmas due to the enhanced coupling of the different m's. Another consequence is that the GAEs which, in a cylinder, are detached from the continuum now lie inside the continua of other toroidally coupled modes. This brings a finite, toroidicity induced continuum damping to the GAEs. We shall see that the GAE continuum damping rates obtained with the cold toroidal model are much higher than the Landau and TTMP damping of GAEs predicted by the hot cylindrical plasma model and are in very good agreement with experiment. We now have an explanation why the GAEs (seen in the experiment as peaks in the antenna loading) are not as sharp as the hot cylindrical model predicts. While the real part of the eigenfrequency of most GAEs is correctly predicted by cylindrical models, there is a noticeable exception: the existence of a GAE just below the $m = 0$ continuum can only be predicted by a toroidal model that includes finite ω/ω_{ci} effects and is in good agreement with experiment [3].

The toroidal effects on the spectrum of Alfvén modes are most dramatic in the lower frequency range. While Eqs (1) and (2) predict reasonably well the position of the Alfvén resonances for cases where the continuum frequencies of different m's are well separated from each other, they fail completely when these become close to each other: toroidal coupling removes the degeneracy of different m's and gaps appear in the continuum. For example, the coupling of m with $m + 1$ creates gaps at rational q magnetic surfaces $q = (|m| + 1/2)/|n|$. The frequencies of the centres of the toroidicity induced gaps are

$R_0\omega/v_{A0} = 1/(2q\sqrt{\rho})$, where ρ is the mass density normalized to its magnetic axis value and v_{A0} is the Alfvén velocity on magnetic axis. To first order in inverse aspect ratio the gap size is proportional to the inverse aspect ratio and the Shafranov shift of the magnetic surface $q = (|m| + 1/2)/|n|$. The plasma elongation couples m to $m + 2$ and ellipticity induced continuum gaps appear near rational q surfaces $q = (|m|+1)/|n|$. The centers of these gaps is given by $R_0\omega/v_{A0} = 1/(q\sqrt{\rho})$. Other gaps are created by the higher order coupling of poloidal wavenumbers m. This gap creation is similar to the formation of forbidden energy bands for an electron in a periodic potential in solid state theory.

Toroidicity and non-circularity have consequences on the spectrum of GAEs. It was shown [16], [17] that GAEs can exist in the toroidicity and ellipticity induced gaps. They have been named TAEs and EAEs or 'gap modes'. The destabilization of TAEs by fast particles in tokamak plasmas predicted by theory [6]-[10] and experimentally observed [11]-[13] has recently revived the interest in Alfvén waves. In the context of fusion-oriented research one should be able to predict as accurately as possible the conditions that can lead to such instabilities and to determine whether the region in parameter space where instabilities are avoided is compatible with the operation of a tokamak reactor.

3 Damping and drive mechanisms

In a plasma consisting of electrons, bulk ions and fast ions several damping and drive mechanisms are at work. The damping mechanisms are :

a) resonance absorption (sometimes called 'continuum damping'), when the TAE eigenfrequency matches a frequency of the Alfvén continuum;

b) electron, bulk ion and fast ion Landau dampings due to the curvature drift and the finite parallel electric field of the wave;

c) transit-time magnetic pumping (TTMP) on electrons, bulk ions and fast ions due to the finite parallel magnetic field of the wave (compressibility).

d) the non-perturbative interaction with the kinetic Alfvén wave [19]: in certain situations the Alfvén eigenmode couples to the KAW which carries the energy away, hence the name 'radiative damping';

e) collisional damping on trapped particles [10].

The instability drive is due to the spatial gradient of the fast ion pressure. Passing particles interact with the wave at the parallel resonance, whereas the wave resonates

with trapped particles at the bounce frequency and its harmonics. In NBI heated plasmas with parallel injection the first type of interaction will dominate. In ICRF minority heated plasmas, most of the high energy tail of the minority ion distribution is in the perpendicular direction to the magnetic field, hence one can expect a substantial number of trapped fast ions and the bounce resonance will dominate. In a fusion reactor the alpha particles will be isotropic and both passing and trapped alphas will be present.

From local theories [6]-[9] we know that three basic conditions must be met for instability:

1 The birth velocity v_0 of fast particles must exceed the parallel phase velocity v_p of the eigenmode so that the fast passing particles can resonantly interact with the eigenmode. Or, for trapped particles, the eigenfrequency must be such that it can resonate with the bounce frequency or its harmonics.

2 The fast particle pressure gradient $|dp_f/dr|$ must exceed a given threshold so that the drift frequency ω^* is larger than the eigenfrequency ω_0 .

3 The fast particle induced growth rate, $|\gamma/\omega|_{fast}$, must exceed the sum of all damping rates, $|\gamma/\omega|_{damp}$.

Theories modelling the wave-particle interaction differ in their basic assumptions: zero order in FLR, second order in FLR or all orders in FLR [24]; finite drift orbit width (FOW) [10]; perturbative dissipative kinetic effects only or non-perturbative; collisional or collisionless interaction only; simplified geometry, expansion in inverse aspect ratio or full toroidal geometry; simplified poloidal mode coupling or coupling to all orders. They differ also in the approach, either local or global. Local theories suffer from a number of shortcomings. For example the TAEs are not localized at a given rational $q = (|m| + 1/2)/|n|$ surface. They extend over the whole plasma cross-section, with wavefield components E_n and B_b peaking at all such rational surfaces and E_b, B_n and $B_{||}$ having a broader radial dependence [18] . Moreover, the eigenfrequencies and eigenmode structures depend on global geometrical parameters such as the shape of the cross-section and equilibrium density and q profiles. Local theories usually use some kind of expansion in geometrical parameters (a/R_0). A more accurate evaluation is needed in order to model actual and future tokamaks.

The expected density profile of fusion alpha particles in a reactor is largely unknown and can only be inferred from theoretical models based on a number of assumptions on transport properties of plasmas yet to be produced. The instability threshold strongly depends on this profile, therefore we must address the question of Alfvén eigenmode stability for a wide range of fast particle density profiles.

The possibility of exciting TAEs when they are stable is currently investigated at JET. The saddle coils now installed in the machine serve as antennas. The planned experiments aim at determining the spectrum of TAEs and their overall linear damping-growth rate by diagnosing the plasma response. Even in the absence of fast particles these experiments will be helpful in studying the damping mechanisms acting on TAEs.

For the study of Alfvén eigenmode stability we adopt a global approach similar to that of Ref. [10]. The eigenmodes are computed globally in true toroidal geometry consistent with an ideal MHD equilibrium. Kinetic effects (damping and driving mechanisms) and fast particles are treated perturbatively. More precisely, we first obtain the global eigenmodes and then use these given eigenmode fields to evaluate the global overall wave-particle power transfer assuming given fast particle density profiles. The marginal stability point is obtained by scaling the number of fast particles so that the overall power transfer is zero. The wave-particle power transfers (to the electrons, bulk ions and fast ions) are evaluated using the drift-kinetic equations (DKE).

4 Models

4.1 Global toroidal zero Larmor radius model

We consider ideal MHD axisymmetric equilibria $\vec{B_0}= T\nabla\varphi + \nabla\varphi \times \nabla\psi$ where T is the toroidal flux function, φ is the toroidal angle and the poloidal flux ψ is a solution of the Grad-Shafranov equation obtained with the bicubic finite element code CHEASE [25] . The plasma is modelled as a cold, current-carrying plasma [26] neglecting electron inertia. In the limit $\omega/\omega_{ci} \rightarrow 0$ it is equivalent to ideal MHD setting the adiabaticity index to zero. The linearized equations for the electric wave field are written in the variational form :

$$\int_{V_p} \left\{ \left| \nabla\times \vec{E} - \vec{J}\, E_b \right|^2 - 2\, \vec{J}\cdot\nabla_{\|}\, \vec{e}_n\, |E_b|^2 - \frac{\omega^2}{c^2}\, \vec{E}^{\star} \cdot \begin{pmatrix} \epsilon_{nn} & \epsilon_{nb} \\ \epsilon_{bn} & \epsilon_{bb} \end{pmatrix} \cdot \vec{E} \right\} d^3x + \int_{V_v} \left| \nabla\times \vec{E} \right|^2 d^3x = 0 \qquad (3)$$

where $\vec{J}= (\mu_0\, \vec{j_0} \times \vec{e_n})/B_0$, $\vec{j_0}$ is the equilibrium current, V_p is the plasma volume and

$$\begin{aligned} \epsilon_{nn} = \epsilon_{bb} &= \frac{c^2}{v_A^2} \sum_i \frac{f_i}{1-(\frac{\omega}{\omega_{ci}})^2}, \\ \epsilon_{nb} = \epsilon_{bn}^{\star} &= i\frac{c^2}{v_A^2} \sum_i \frac{f_i \omega/\omega_{ci}}{1-(\frac{\omega}{\omega_{ci}})^2}, \\ f_i &= \frac{n_i m_i}{\sum_j n_j m_j}. \end{aligned} \qquad (4)$$

The plasma is surrounded by a vacuum region V_v enclosed by a perfectly conducting wall. In the vacuum region an antenna is modelled by an infinitely thin sheet $D(\vec{x})$ on which currents $\vec{j_a}$ of given frequency ω and toroidal mode number n are prescribed :

$$\vec{j_a} = \delta(D)\nabla D \times \nabla\alpha \tag{5}$$

$$\alpha = \sum_n \alpha_n(\theta) \exp i(n\varphi - \omega t) \tag{6}$$

where θ is the poloidal angle. The coefficients α_n are obtained from the Fourier series decomposition of the actual antenna currents. We have the possibility to model helical antennas, 'top/bottom' antennas of the TCA type, low or high field side (LFS or HFS) antennas and saddle coil antennas that are installed in JET. Different phasings of the antenna currents give different toroidal Fourier spectra α_n. It is thus possible to select the desired mode numbers n.

Special care must be taken because of the existence of the Alfvén continuous spectrum. We add a small imaginary part to the dielectric tensor in Eq.(3): ω is replaced by $\omega(1 + i\nu)$, with $\nu > 0$ to ensure causality. The operator in Eq.(3) is now regular and can be solved numerically but has lost its hermiticity. The limit $\nu \to 0$ is extrapolated from the numerical results of the LION code and gives a finite damping rate if the wave frequency is in the Alfvén continuum. Second, the discretization scheme must avoid spectral pollution. The use of hybrid elements in the LION code ensures that [18], [26].

The variational form (3) is written in toroidal axisymmetric geometry using a toroidal magnetic coordinate system (ψ, χ, φ) where χ is a general poloidal coordinate, and discretized with finite hybrid elements in the plasma domain. The vacuum, including the antenna, is solved with a Green's function technique. The LION code computes the wave-field solution of Eq.(3) and the total absorbed power P for given antenna frequencies ω. A global mode shows as a peak on $P(\omega)$ [18].

4.2 Global toroidal kinetic model for the wave-particle power transfers

The evolution equation used for the plasma species is the Drift Kinetic Equation (DKE)

$$\frac{Df}{Dt} = \left[\frac{\partial}{\partial t} + \vec{v_g} \cdot \frac{\partial}{\partial \vec{X}} + \frac{d\epsilon}{dt}\frac{\partial}{\partial \epsilon} + \frac{d\mu}{dt}\frac{\partial}{\partial \mu}\right] f(\vec{X}, \epsilon, \mu, t) = 0, \tag{7}$$

where $\vec{X}$ is the guiding center, $\epsilon = \frac{1}{2}(v_{||}^2 + v_\perp^2)$, $\mu = v_\perp^2/2B_0$, $\vec{v_g} = v_{||}\,\vec{e}_B + \vec{v_E} + \vec{v_d}$, $\vec{v_E} = \vec{E} \times (\vec{B_0} + \vec{B})/B^2$, $\vec{v_d} = (m/qB)\,\vec{e}_B \times \left(v_\perp^2/2 + v_{||}^2\right) \nabla \ln B$, $B = |\,\vec{B_0} + \vec{B}\,|$, $(\vec{E}, \vec{B})$ are the perturbing electromagnetic fields and $\vec{e}_B = (\vec{B_0} + \vec{B})/B$.

Equation (7) is first solved to obtain a stationary distribution function. To lowest order in the Larmor radius expansion one obtains

$$F = F(\psi, \epsilon, \mu). \tag{8}$$

In particular for electrons and bulk ions a local Maxwellian distribution is chosen

$$F = \frac{N(\psi)}{(\pi v_{th}^2(\psi))^{3/2}} \exp\left(-2\frac{\epsilon}{v_{th}^2(\psi)}\right), \tag{9}$$

with density N and thermal velocity squared $v_{th}^2 = 2T/m$. For the fast particles a slowing-down distribution is assumed [27]

$$F = N(\psi)\frac{C(\psi)}{v^3 + v_c^3(\psi)} H(v_0 - v), \tag{10}$$

$$v_c = \left(3\sqrt{\pi}\frac{m_f + m_i}{m_f m_i} m_e\right)^{1/3} \left(\frac{T_e}{m_e}\right)^{1/2}, \tag{11}$$

$$C = \frac{3}{4\pi \ln\left[\left(\frac{v_0}{v_c}\right)^3 + 1\right]}, \tag{12}$$

where H is the Heaviside function and v_0 the birth velocity of the fast particles ($v_0 = 1.3 \cdot 10^7 m/s$ for fusion alphas).

The linearized DKE is then solved to obtain the fluctuating part of the distribution function $\tilde{f}$ in terms of the EM fields. The operator $\vec{v_d} \cdot \nabla$ is considered as a perturbation $\mathcal{O}(\varepsilon)$. The linearized DKE is solved to second order in ε and only the most dominant elements among comparable terms are retained. Furthermore, to avoid an integration along the field line, the differential operator $\vec{e}_{||} \cdot \nabla$, is replaced by its magnetic-surface-averaged value $< \nabla_{||} >= ik_{||}$, where

$$k_{||}^2 = \frac{\oint_{\psi=const} dl \left(|\nabla_{||} E_n|^2 + |\nabla_{||} E_b|^2\right)}{\oint_{\psi=const} dl |\vec{E}|^2}, \tag{13}$$

The integrals in Eq.(13) are evaluated along a closed path in the poloidal plane on a $\psi = const$ surface. Instead of using Eq. (13), one could make the rough approximation $k_{||}^2 = \omega^2/v_A^2$ for Alfvén waves; but $k_{||}$ obtained in this way can be wrong by a factor up to 3 for TAEs because of the toroidal coupling. The solution of the linearized DKE can then be written as

$$\begin{aligned} \tilde{f} = \frac{-iq}{m\omega_c\Omega_0} \Big\{ & \frac{1}{\omega}\left(\Omega_0 E_b - iv_{||}\nabla_p E_{||}\right)\nabla_n F \\ & + \left[\omega_c v_{||} E_{||} + \left(\frac{v_\perp^2}{2} + v_{||}^2\right)\vec{\beta}_\perp \cdot \vec{E} - i\omega\frac{v_\perp^2}{2} B_{||}\right]\frac{\partial F}{\partial \epsilon} \\ & - i\frac{1}{\omega\omega_c}\left(\frac{v_\perp^2}{2} + v_{||}^2\right)(\vec{\beta}_\perp \cdot \nabla) E_b \nabla_n F \Big\}, \end{aligned} \tag{14}$$

where $\omega_c = qB_0/m$, $\Omega_0 = \omega + i\eta - k_{||}v_{||}$, with $\eta > 0$ to ensure causality, $\vec{\beta}_\perp = \left(\nabla \times \vec{e}_{||}\right)_\perp$ and $\nabla_p = (\nabla\varphi \times \nabla\psi)/|\nabla\varphi \times \nabla\psi| \cdot \nabla$.

One can now derive the power absorption formula. The total power exchanged between the particles and the perturbing EM fields averaged over time reads

$$P_{species} = \frac{1}{2}\Re e \int d\Gamma \, \frac{\tilde{d\epsilon}}{dt} \tilde{f}^*_{species}, \qquad d\Gamma = d^3X d^3v. \tag{15}$$

We retain only the resonant contribution to $P_{species}$. Writing $P_{species} = P^{homo}_{species} + P^{inhomo}_{species}$ we obtain for a Maxwellian distribution

$$\begin{aligned} P^{homo} &= \sqrt{\pi}\epsilon_0 \int d^3x \frac{\omega_p^2 v_{th}}{4\omega_c^2 |k_{||}|} \exp(-z_0^2) \times \\ &\left\{ \left| 2z_0 \frac{\omega_c}{v_{th}} E_{||} + \left(1 + 2z_0^2\right) \vec{\beta}_\perp \cdot \vec{E} - i\omega B_{||} \right|^2 + \left| \vec{\beta}_\perp \cdot \vec{E} - i\omega B_{||} \right|^2 \right\}, \end{aligned} \tag{16}$$

$$\begin{aligned} P^{inhomo} &= \sqrt{\pi}\epsilon_0 \Im m \int d^3x \nabla'_n \frac{\omega_p^2 v_{th}^3}{8\omega\omega_c^3 |k_{||}|} \exp(-z_0^2) \left\{ \left[2z_0 \frac{\omega_c}{v_{th}} E_{||} + \left(1 + 2z_0^2\right) \vec{\beta}_\perp \cdot \vec{E} - i\omega B_{||} \right] \times \right. \\ &\left. \left[\left(1 + 2z_0^2\right) (\vec{\beta}_\perp \cdot \nabla E_b^*) + 2z_0 \frac{\omega_c}{v_{th}} \nabla_p E_{||}^* \right] + \left[\vec{\beta}_\perp \cdot \vec{E} - i\omega B_{||} \right] (\vec{\beta}_\perp \cdot \nabla) E_b^* \right\}, \end{aligned} \tag{17}$$

where $\omega_p^2 = Nq^2/m\epsilon_0$, $z_0 = \omega/k_{||}v_{th}$ and ∇'_n is equivalent to ∇_n except that it operates only on density and temperature. For the slowing-down distribution we obtain

$$\begin{aligned} P^{homo} &= \pi^2 \epsilon_0 \int d^3x \frac{\omega_p^2 C}{|k_{||}|} \left\{ \frac{1}{|v_p|^3 + v_c^3} \left| v_p E_{||} + \frac{1}{\omega_c} v_p^2 \vec{\beta}_\perp \cdot \vec{E} \right|^2 \right. \\ &\left. + \frac{2I_0}{\omega_c} \Re e \left(\vec{\beta}_\perp \cdot \vec{E}^* + i\omega B_{||}^* \right) \left(v_p E_{||} + \frac{v_p^2}{\omega_c} \vec{\beta}_\perp \cdot \vec{E} \right) + \frac{I_1}{\omega_c^2} \left| \vec{\beta}_\perp \cdot \vec{E} - i\omega B_{||} \right|^2 \right\}, \end{aligned} \tag{18}$$

$$\begin{aligned} P^{inhomo} &= -\pi^2 \epsilon_0 \Im m \int d^3x \nabla'_n \frac{\omega_p^2 C}{|k_{||}|\omega_c} \left\{ I_0 \left(v_p E_{||}^* + \frac{v_p^2}{\omega_c} \vec{\beta}_\perp \cdot \vec{E}^* \right) \left(\frac{v_p^2}{\omega\omega_c} (\vec{\beta}_\perp \cdot \nabla) E_b + \frac{\nabla_p E_{||}}{k_{||}} \right) \right. \\ &+ \frac{I_1}{2\omega_c} \left[\left(\vec{\beta}_\perp \cdot \vec{E}^* + i\omega B_{||}^* \right) \left(\frac{v_p^2}{\omega\omega_c} (\vec{\beta}_\perp \cdot \nabla) E_b + \frac{\nabla_p E_{||}}{k_{||}} \right) \right. \\ &\left. \left. + \frac{1}{\omega} (\vec{\beta}_\perp \cdot \nabla) E_b \left(v_p E_{||}^* + \frac{v_p^2}{\omega_c} \vec{\beta}_\perp \cdot \vec{E}^* \right) \right] + \frac{I_2}{4\omega\omega_c^2} (\vec{\beta}_\perp \cdot \nabla) E_b \left(\vec{\beta}_\perp \cdot \vec{E}^* + i\omega B_{||}^* \right) \right\}, \end{aligned} \tag{19}$$

$$\text{where} \quad I_n = \int_{|v_p|}^{v_0} dv \frac{v \left(v^2 - v_p^2\right)^n}{v^3 + v_c^3}. \tag{20}$$

The EM fields are obtained from a global wave solution. If we use the zero order Larmor radius model of Section 4.1, in which $E_{||}$ is approximated by zero, $E_{||}$ must be obtained

from a more general model. The starting point is the quasi-neutrality condition $\tilde{N}_e = \tilde{N}_i$. As the thermal velocity of the electrons can be comparable to the parallel phase velocity ($v_{the} \sim |v_p|$), it is reasonable to evaluate $\tilde{N}_e$ using a kinetic model. Integrating $\tilde{f}_e$ over velocity leads to

$$\tilde{N}_e = 2i\frac{eN_e}{m_e\omega\omega_{ce}}\left[\frac{\omega\omega_{ce}}{k_\parallel v_{the}^2}(1-Z)\,E_\parallel - \frac{1}{2}Z\left(\vec{\beta}_\perp\cdot\vec{E}_\perp - i\omega B_\parallel\right) + \left(\frac{\omega}{k_\parallel v_{the}}\right)^2(1-Z)\,\vec{\beta}_\perp\cdot\vec{E}\right], \tag{21}$$

where $Z \equiv Z\left(\frac{\omega}{|k_\parallel|v_{the}}\right)$ is the plasma dispersion function [28]. To evaluate $\tilde{N}_i$ one can use a cold fluid model for the ions as $v_{thi} \ll |v_p|$. Due to their relatively large mass, the ions dominate the motion perpendicular to the magnetostatic field. Solving the equation of motion in the perpendicular plane, one obtains for low frequencies $\omega \ll \omega_{ci}$

$$\vec{v} = \frac{e}{m_i\omega_{ci}}\left[\vec{E}_\perp \times \vec{e}_\parallel - i\frac{\omega}{\omega_{ci}}\vec{E}_\perp\right], \tag{22}$$

and using the equation of continuity for the ion density gives

$$\tilde{N}_i = -\frac{eN_i}{m_i\omega_{ci}^2}\left[\nabla\cdot\vec{E}_\perp - 2i\frac{\omega_{ci}}{\omega}\vec{\beta}_\perp\cdot\vec{E}_\perp - \omega_{ci}B_\parallel\right]. \tag{23}$$

Inserting these density relations in the quasi-neutrality condition leads to

$$E_\parallel = -\frac{k_\parallel v_{the}^2}{2\omega\omega_{ce}}\left\{\frac{1}{1-Z}\left(i\frac{\omega}{\omega_{ci}}\nabla\cdot\vec{E}_\perp + \vec{\beta}_\perp\cdot\vec{E}_\perp\right) + \left[1+2\left(\frac{\omega}{k_\parallel v_{the}}\right)^2\right]\vec{\beta}_\perp\cdot\vec{E}_\perp - i\omega B_\parallel\right\}. \tag{24}$$

Finally, using the above expression in Eq.(16) for electrons and bulk ions gives

$$P^{homo} = \sqrt{\pi}\epsilon_0\int d^3x\frac{\omega_p^2 v_{th}}{4\omega_c^2|k_\parallel|}\exp -z_0^2 \times \left(|a_{species}|^2 + \left|\vec{\beta}_\perp\cdot\vec{E} - i\omega B_\parallel\right|^2\right), \tag{25}$$

$$a_{electron} = \frac{1}{1-Z}\left(i\frac{\omega}{\omega_{ci}}\nabla\cdot\vec{E}_\perp + \vec{\beta}_\perp\cdot\vec{E}_\perp\right), \tag{26}$$

$$\begin{aligned} a_{ion} = {} & \frac{T_e}{T_i}\frac{1}{1-Z}\left(i\frac{\omega}{\omega_{ci}}\nabla\cdot\vec{E}_\perp + \vec{\beta}_\perp\cdot\vec{E}_\perp\right) - i\omega\left(1+\frac{T_e}{T_i}\right)B_\parallel \\ & + \left[1+\frac{T_e}{T_i}+2\left(\frac{\omega}{k_\parallel v_{thi}}\right)^2\right]\vec{\beta}_\perp\cdot\vec{E}_\perp . \end{aligned} \tag{27}$$

P^{inhomo} can be neglected for these species. This is related to the fact that in the frame of the present work $\omega \gg \omega^*$ for electrons and bulk ions, where ω^* is the characteristic frequency of the drift mode. Note that the contributions of $E_\parallel$ to the ion power absorption

are proportional to T_e/T_i. As the average kinetic energy of the fast particles is very high as compared with the energy of the electrons, the contributions of $E_{||}$ to the power absorbed by the fast particles can therefore be neglected. In this way, one can write for the fast particles

$$P_f^{homo} = \pi^2\epsilon_0 \int d^3x \frac{\omega_{pf}^2 C}{|k_{||}|\omega_{cf}^2} \left\{ \left[\frac{v_p^4}{|v_p|^3 + v_c^3} + 2v_p^2 I_0 \right] \left| \vec{\beta_\perp} \cdot \vec{E} \right|^2 \right. \\ \left. + 2\omega v_p^2 I_0 \Im m \left(B_{||} \, \vec{\beta_\perp} \cdot \vec{E}^* \right) + I_1 \left| \vec{\beta_\perp} \cdot \vec{E} - i\omega B_{||} \right|^2 \right\}, \tag{28}$$

$$P_f^{inhomo} = \frac{\pi^2\epsilon_0}{\omega} \Im m \int d^3x \nabla'_n \frac{\omega_{pf}^2 C}{|k_{||}|\omega_{cf}^3} \left\{ \left(v_p^4 I_0 + v_p^2 \frac{I_1}{2} \right) \vec{\beta_\perp} \cdot \vec{E} \right. \\ \left. + \left(v_p^2 \frac{I_1}{2} + \frac{I_2}{4} \right) \left(\vec{\beta_\perp} \cdot \vec{E} - i\omega B_{||} \right) \right\} (\vec{\beta_\perp} \cdot \nabla) E_b^*. \tag{29}$$

The expressions (25)-(29) have been written in toroidal axisymmetric geometry and implemented in the LION code. Marginal stability is reached when the sum of the DKE powers of the different species $P_{species}$ is zero. Note that the mode is always stable (i.e. stable for any fast particle density) if $P_f^{homo} + P_f^{inhomo} > 0$. Thus instead of the necessary instability criterion of local theories, $\omega - \omega^* < 0$, we have the necessary global instability criterion $P_f^{homo} + P_f^{inhomo} < 0$. More details about the derivation of the DKE powers can be found in Ref.[29].

4.3 Global toroidal finite Larmor radius model

The global perturbative approach developed in the previous two subsections fails when the eigenmode interacts with the KAW or the SQEW: the wavefields obtained with the zero Larmor radius model are dramatically modified when a kinetic wave is present. This happens for example when a global eigenmode has an eigenfrequency that crosses that of an Alfvén continuum. The wavefields cannot be obtained with a perturbative approach because the inclusion of FLR terms in the equations is a singular perturbation of the zero order ones. A global wave FLR model in 1-D geometry was already developed [22]. For the study of TAEs, however, the toroidal geometry must be included in the description. We describe here recent developments in this field.

The hot plasma dielectric tensor operator $\vec{\vec{\epsilon}}$ in toroidal axisymmetric geometry was derived in Ref.[30]. This operator includes FLR effects up to second order in $k_\perp \rho_{Li}$ and equilibrium gradients effects up to first order in ρ_{Li}/L_{eq}, where $k_\perp$ is a differential operator in the perpendicular direction to the magnetic field, ρ_{Li} is the ion Larmor radius

and L_{eq} is the equilibrium scale length. Instead of solving for the wave electric field

$$\nabla \times \nabla \times \vec{E} - \frac{\omega^2}{c^2} \vec{\vec{\epsilon}} \; \vec{E} = i\omega\mu_0 \vec{j}_a, \tag{30}$$

where $\vec{j}_a$ is the antenna current density, we use the vector and scalar potentials $\vec{A}$ and ϕ. The Coulomb gauge is chosen and the equations can then be written as [31]

$$\begin{cases} \nabla^2 \vec{A} + \frac{\omega^2}{c^2} \vec{\vec{\epsilon}} \; \vec{A} + \frac{i\omega}{c^2} \vec{\vec{\epsilon}} \; \nabla\phi & = & -\mu_0 \vec{j}_a \\ \nabla \cdot \left(\vec{\vec{\epsilon}} \; \nabla\phi \right) - i\omega \nabla \cdot \left(\vec{\vec{\epsilon}} \; \vec{A} \right) & = & 0 \end{cases} \tag{31}$$

The condition $\nabla \cdot \vec{A} = 0$ is imposed on the domain boundaries. In order to simplify the unicity conditions on the magnetic axis, we set $\phi = 0$ there.

Eq.(31), with $\vec{\vec{\epsilon}}$ from Ref.[30], is projected on the orthonormal set $(\vec{e}_n, \vec{e}_b, \vec{e}_{\|})$ defined in section 2 and is written in a weak variational form in toroidal magnetic coordinates (s, θ, φ), where $s = \sqrt{\psi/\psi_s}$, ψ_s is the value of ψ at the plasma surface, θ is the poloidal angle and φ is the toroidal angle. Partial integrations are performed so as to satisfy the regularity of the solution on axis. The equations are then discretized with Hermite bicubic finite elements. More details can be found in Ref.[32] about the numerical procedure and the validation of the code (PENN). This work is still in progress and we report below on some results. Another possibility is to use a poloidal Fourier decomposition of the wavefields and solve for the electric field [5].

Note that the DKE powers derived in Section 4.2 can be used with the wavefields of the FLR model. Unlike the zero Larmor radius model of Section 4.1 the wave parallel electric field $E_{\|}$ is consistently calculated. So instead of Eqs.(25)- (29) we can use Eqs.(16)-(19). With this model the stability of Alfvén eigenmodes including the interaction with the KAW described consistently (non-perturbatively) can be studied. The radiative damping, mode conversion and kinetic eigenmodes (e.g. 'KTAE') are described by this model.

5 Excitation of Alfvén waves with an antenna

5.1 AWH in TCA

As an illustration of a possible AWH scenario we examine the case of the TCA tokamak [1]-[3]. It is a small machine with a circular cross-section. Its main parameters are: $R_0 = 0.61m$, $a = 0.18m$, $B_0 = 1.5T$; typical densities on axis are in the range $n_{D0} = 1 - 10 \times 10^{19} m^{-3}$, and in the usual mode of operation the presence of sawteeth indicates q_0 close to 1 or lower. The antenna consists of four pairs of straps placed above and below the plasma column at four equidistant toroidal locations. With different relative

Figure 1: *Level line plots for $Re(E_n)$ using the LION code (zero Larmor radius model). The parameters correspond to the TCA tokamak with $f = 2.45MHz, n = -2, q_0 = 1.05, q_a = 2.66, B_0 = 1.5T, n_D = 5.2 \times 10^{19} m^{-3}(1 - 0.6s^2)$*

phasings of the straps different n's are excited. The toroidal Fourier decomposition of these antennas is rather pure. In its standard phasing configuration $n = \pm 2$ are the dominant components. The antenna generator frequency can be varied in the range $1 - 5MHz$. The plasma density is observed to rise significantly during AWH, indicating a substantial effect of AWH on particle confinement or recycling. The parameters were chosen such as to excite the surface mode and to have an Alfvén resonance surface close to the magnetic axis.

We show in Fig.1 the contour plot of $Re(E_n)$ for $n = -2$, a helical antenna $m = -1$, a density profile $n_D = 5.2 \times 10^{19} m^{-3}(1 - 0.6s^2)$, $q_0 = 1.05$, $q_a = 2.66$. The LION code (toroidal zero Larmor radius model, Section 4.1) was used with $\nu = 0.01$. The large edge pedestal in density and the low q implies that only two main Alfvén resonances are present in the plasma, at $s = 0.35$ and at $s = 0.915$. The inner one has $m = -1$ dominant, as the cylindrical model would predict, and the outer one is a toroidally coupled surface which, in a cylinder, would be the $m = 0$ but here shows a broad m spectrum with dominant numbers $m = +1, -1, +2, +3$ and 0. The external surface absorbs about 20% of the total power, which means that about 80% of the power is deposited near the centre. This is, however, very optimistic: with more realistic density profiles there are many more

Figure 2: *Level line plots for $Re(E_n)$ using the PENN code (FLR model). The parameters are the same as in Fig.1, with $T_e(s) = 400eV(1 - 0.98s^2)^2$, $T_i(s) = 100eV(1 - 0.98s^2)^2$.*

resonance surfaces near the edge. Moreover, the $n = +2$ component, also present in the antenna excitation, has Alfvén resonances closer to the edge. As a result, computations with the LION code show that it is difficult to deposit more than 50% of the wave energy inside half the minor radius.

We now consider the same case but use the toroidal second order FLR model described in Section 4.3. The electron and ion temperatures were chosen as $T_e(s) = 400eV(1 - 0.98s^2)^2$ and $T_i(s) = 100eV(1 - 0.98s^2)^2$. The contour plot of $Re(E_n)$ is shown in Fig.2. Two main differences appear as compared to the zero Larmor radius model. First, a KAW is present between the former Alfvén resonance at $s = 0.35$ and the magnetic axis. The value of $\omega/(k_{\|}v_{te})$ is 0.41 at s=0.35: mode conversion to the KAW occurs as expected. The KAW can form a standing wave and this may correspond to the 'satellite' peak seen in the TCA experiment [2]. It has no equivalent in the zero order FLR model. Second, the former Alfvén resonance at $s = 0.915$ is replaced by mode conversion to a SQEW propagating outwards: at $s = 0.915$, $\omega/(k_{\|}v_{te}) = 1.6$. At $s = 0.81$, a small amplitude $m = 7$ structure is present. It corresponds to an Alfvén resonance surface that is also present in the zero Larmor radius computation. (It does not show up on the wavefield plot of Fig.1 because of its relatively smaller amplitude). The FLR calculation shows no

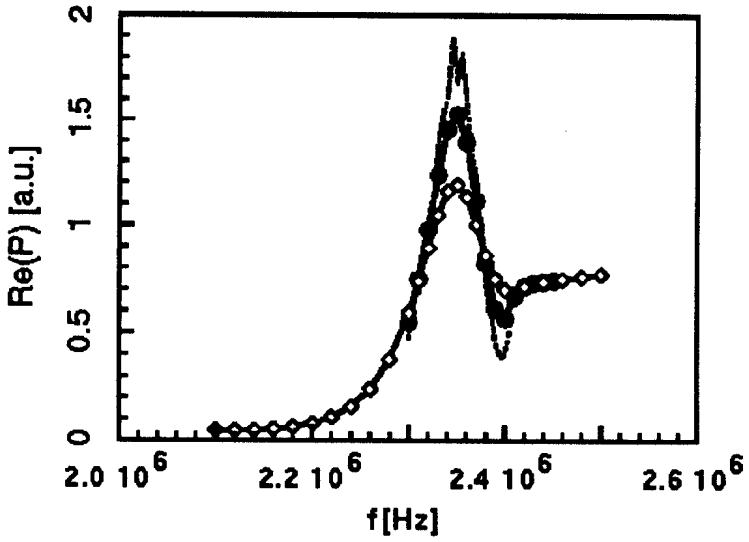

Figure 3: *Resistive antenna power load vs frequency for* $\nu = 0.01$ *(open symbols),* $\nu = 0.005$ *(filled symbols) and* $\nu = 0.0025$ *(dotted line), using the LION code. The parameters are typical of the TCA tokamak:* $f = 2.365MHz, n = -2, q_0 = 1.05, q_a = 4.55, B_0 = 1.5T, n_D = 5.2 \times 10^{19} m^{-3}(1 - 0.98s^2)^{0.7}$

mode conversion there: the reason is that $\omega/(k_{||}v_{te})$ is close to unity there and electron Landau damping is large. As the power absorption diagnostics are not yet implemented in the PENN code, we cannot tell which fraction of energy is deposited near the centre. The code computes the total power in two different ways: the power dissipated at the antenna and the Poynting flux at the plasma-vacuum interface. With a mesh consisting of 31 radial intervals and 28 poloidal intervals in the plasma, the consistency of these powers is verified with an accuracy better than 0.5%.

5.2 GAEs in TCA

In the TCA experiment, the density rise during AWH had the consequence that the Alfvén spectrum was scanned during a discharge even though the generator frequency was not swept. Peaks in the resistive antenna impedance appeared at specific values of density [2]. These values were in most cases corresponding to the GAEs as predicted by cylindrical models, with the exception of the $m = 0$ case already discussed in Section 2. The puzzle was the order of magnitude discrepancy in the damping rate of these modes: FLR models in a cylinder predict $|\gamma/\omega|_{damp}$ of the order of 10^{-3} [22], whereas the experimental values are typically of the order of 10^{-2} [2].

Let us consider a TCA plasma with the same parameters as in the previous section except $q_a = 4.55$ and a density profile $(1 - 0.98s^2)^{0.7}$. The generator frequency is scanned

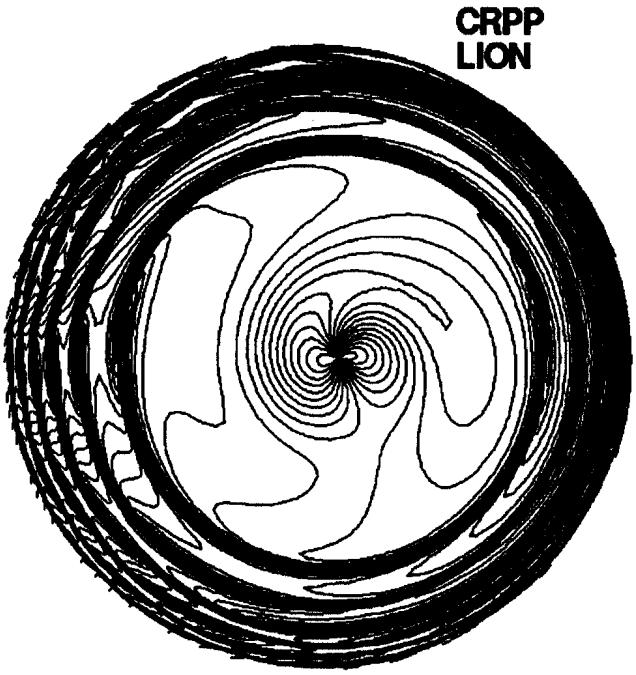

Figure 4: *A GAE in the TCA tokamak. Level line plots for* $Re(E_n)$ *using LION. The parameters are* $f = 2.365MHz, n = -2, q_0 = 1.05, q_a = 4.55, B_0 = 1.5T, n_D = 5.2 \times 10^{19} m^{-3}(1 - 0.98s^2)^{0.7}$

around $2.4Mhz$. As in the experiment, a peak in the antenna loading appears (Fig.3). Measuring its width and taking the limit $\nu \to 0$, we obtain $|\gamma/\omega|_{damp} = 1.0 \times 10^{-2}$, which is in close agreement with the experiment. The explanation for this result can be understood from Fig.4 which shows a contour plot of $Re(E_n)$ for the frequency $f = 2.365Mhz$. In the center of the plasma there is a $m = -1$ structure that is similar to the cylindrical model prediction [20] except that it does not extend up to the plasma boundary but is much more localized inside. In the outer regions several Alfvén resonances are present, at $s = 0.79, 0.88, 0.93, 0.956, 0.975, 0.989$. They are toroidally coupled surfaces. (The cylindrical expression (Eqs(1),(2)) predicts positions of Alfvén resonances at $s = 0.82, 0.90, 0.94, 0.966, 0.982, 0.994$ for $m = 0, 1, 2, 3, 4, 5$, respectively. The actual wavefields in torus show instead a rather broad m spectrum). At each of these surfaces, resonance absorption occurs. This is the origin of the GAE damping rate. Fig.4 also explains the difficulty in depositing the power in the centre of the discharge, due to the large number of toroidally coupled resonance surfaces. This number increases with increasing q: from Eqs (1) and (2) we see that the continuum frequencies of different m's are close to

Figure 5: *Level line plots for $Re(E_n)$ using LION. The parameters correspond to the Phaedrus-T tokamak with $f = 7MHz, n = -7, q_0 = 1.5, q_a = 3.8, B_0 = 0.7T, n_{H0} = 0.3 \times 10^{19} m^{-3}$*

each other at high q. Small aspect ratio and shaping of the plasma cross-section enhance the coupling between m's and it becomes increasingly difficult to deposit the power near the center.

5.3 Alfvén waves in Phaedrus-T

Phaedrus-T is a small tokamak with main parameters $R_0 = 0.92m$, $a = 0.26m$, $B_0 = 0.6 - 0.95T$, $I_p = 20 - 90kA$, no sawteeth ($q_0 > 1$). One of the aims of the current research experimental programme is the study of current drive in the Alfvén frequency range [5]. The density is small for these CD studies, typically $n_{H0} = 0.3 \times 10^{19} m^{-3}$. The antenna consists of two poloidal straps on the LFS of the plasma at toroidal locations separated by $0.14m$. The frequency is $f = 7Mhz$ which, for $B_0 = 0.7T$, is just below the hydrogen cyclotron frequency. The toroidal mode number excitation spectrum of this antenna is rather broad: typically, at least 10 different n's are excited. The phase difference between the two straps can be controlled and thus different toroidal spectra can be launched.

This is a very different regime as compared with the TCA experiment. With the large ω/ω_{ci} and high q one can expect a large number of Alfvén resonance surfaces to

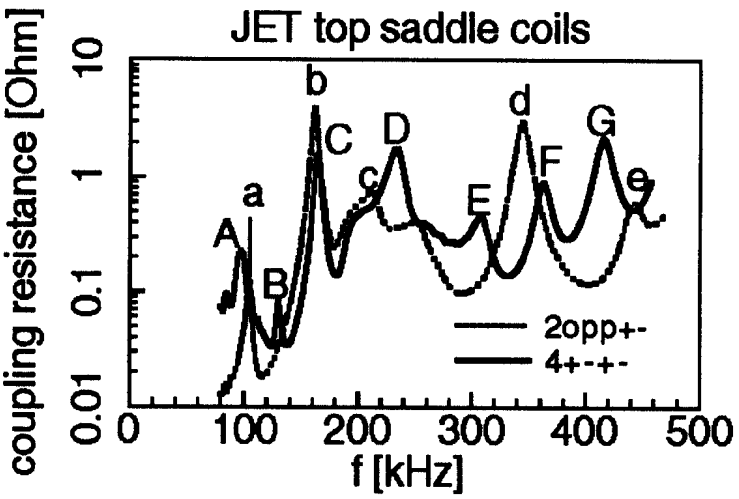

Figure 6: *JET saddle coils resistive coupling computed with the LION code for two possible antenna phasings: two top antennas with (+,-) phasings (dotted line) and four top antennas with (+,-,+,-) phasings. The labels a,b,c,d,e correspond to* $n = 1$ *modes and A,B,C,D,E,F,G to* $n = 2$ *modes. The plasma parameters are* $R_0 = 3m$, $B_0 = 3.45T$, $n_{D0} = 5 \times 10^{19} m^{-3}$, $\nu = 10^{-2}$, $q_0 = 1.1$, $q_a = 3.34$, $I_p = 5MA$, $< \beta >= 3.9\%$, $\beta_{pol} = 0.78$, $a/R = 0.36$, $\kappa = 1.63$. *Note that* $f = 400kHz$ *corresponds to a normalized frequency* $R_0\omega/v_{A0} = 1$.

be excited. This is confirmed by LION code calculations: for $n = -7$, $f = 7Mhz$, $B_0 = 0.7T$, $n_{H0} = 0.3 \times 10^{19} m^{-3}$, $q_0 = 1.5$, $q_a = 3.8$, we show in Fig.5 a contour plot of $Re(E_n)$. A considerable number of resonance surfaces show up. We made a toroidal Fourier scan $n = -15$ to $+15$. The $n = -7$ case is the best case for the power deposition profile and has a reasonable antenna coupling: 38% of the total power is absorbed inside half the minor radius. Summing the toroidal Fourier components we obtain the antenna coupling resistance R_a for various phase differences Δ between the straps: $R_a = 0.165\ \Omega$ for $\Delta = 0$, $R_a = 0.093\ \Omega$ for $\Delta = \pi/2$, $R_a = 0.089\ \Omega$ for $\Delta = -\pi/2$ and $R_a = 0.018\ \Omega$ for $\Delta = \pi$. This is in agreement with the Phaedrus-T experiment.

5.4 TAEs and EAEs in JET

We consider an up-down asymmetric equilibrium configuration typical of a 'single-null' discharge in JET. The parameters are: $a/R_0 = 0.36$, $\kappa = 1.63$, $q_0 = 1.1$, $q_a = 3.34$, $p'(\psi) = 2/3$ of ballooning optimized $p'(\psi)$ profile, $I_p = 5MA$, $< \beta >= 3.9\%$, $\beta_{pol} = 0.78$. For all equilibria considered in this section we keep the same shape of cross-section, value of q_0 and $I^*(\psi)$ profile, where I^* is the magnetic-surface-averaged toroidal current density. Different equilibria are obtained by scaling the $p'(\psi)$ profile.

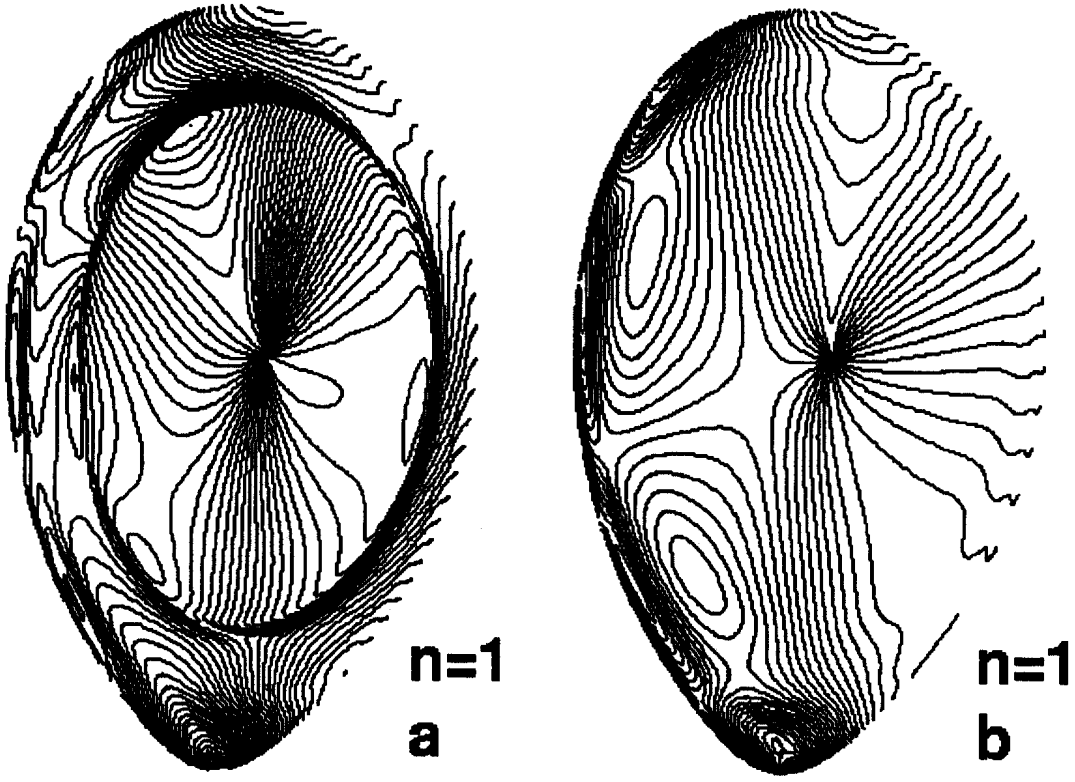

Figure 7: *Contour plots of the real part of the binormal component of the wave electric field, $Re(E_b)$, of the internal (left) and external (right) $n = 1$ TAEs corresponding to the peaks labelled 'a' and 'b' in Fig.6. The normalized frequencies $R_0\omega/v_{A0}$ are 0.2626 (left) and 0.4048 (right).*

We first evaluate the plasma response to the antenna excitation at various frequencies in the absence of kinetic effects. Fig.6 shows the saddle coil antenna coupling resistance for the case $< \beta >= 3.9\%$ and for two different possible antenna phasings. Saddle coils excite TAEs in the frequency range $f = 80 - 250kHz$ and EAEs in the frequency range $f = 250 - 500kHz$. The different modes have very different couplings and this is due to different eigenmode structures. The electric field component $Re(E_b)$ of some TAEs is shown in Figs.7 and 8. There are 'internal' modes, such as the $n = 1$ mode labelled 'a', with a relatively modest wave amplitude at the plasma boundary; therefore the antenna couples weakly to this mode. There are 'external' modes, such as the $n = 1$'b', the $n = 2$'C' and the $n = 3$ modes. Their amplitude is large throughout the plasma cross-section and therefore couple well to an antenna. The $n = 2$ and $n = 3$ external modes have a small amplitude near the magnetic axis: the dominant poloidal mode numbers at $q = 5/4$ and $q = 7/6$ are $m = 2, 3$ and $m = 3, 4$, respectively, and these components

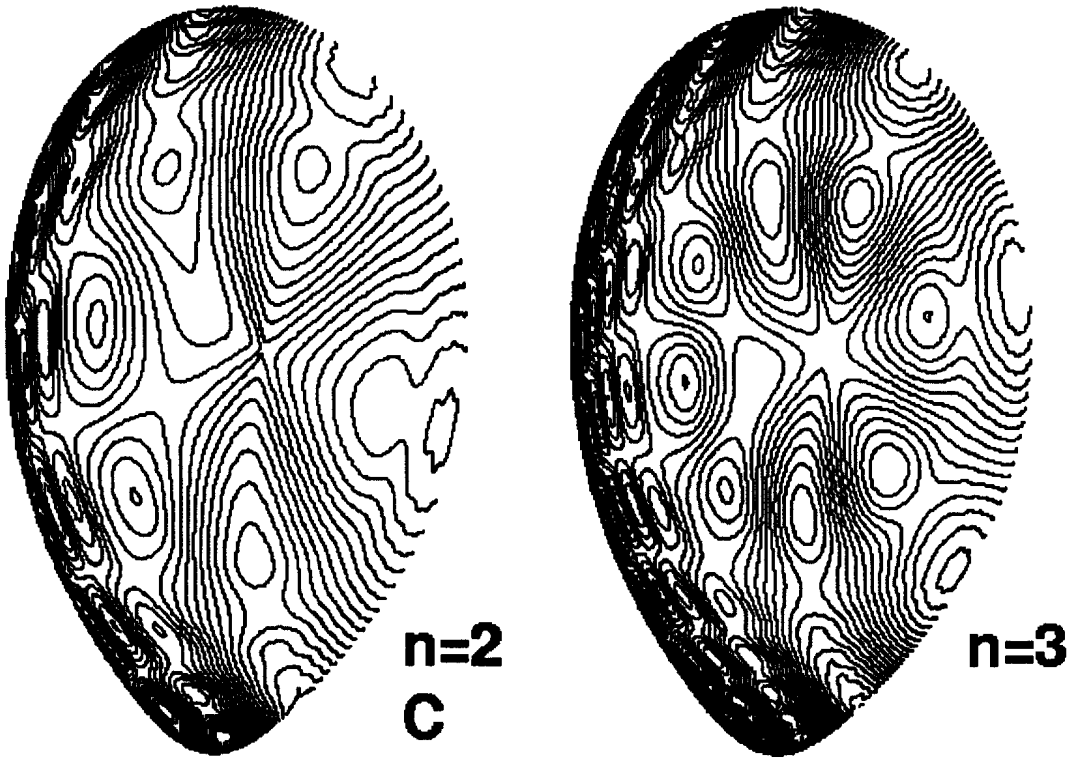

Figure 8: *Contour plots of $Re(E_b)$ of the $n = 2$ (left) and $n = 3$ (right) external TAEs for the same parameters as in Fig.6. The $n = 2$ mode corresponds to the peak labelled 'C' in Fig.6. The normalized frequencies $R_0\omega/v_{A0}$ are 0.4084 (left) and 0.4354 (right).*

tend to vanish at the magnetic axis. This is not the case for the $n = 1$ mode which has $m = 1, 2$ as dominant poloidal mode numbers between the magnetic axis and the $q = 1.5$ surface. The $m = 1$ component is finite at the magnetic axis. The TAEs studied in Refs [16], [7], [10], [33] are 'internal' modes.

There is an interesting difference between internal and external modes. Fig.9(top) shows the eigenfrequencies of the $n = 1$ modes 'a' and 'b' for a sequence of equilibria with varying pressure. The mode 'a' hardly changes its eigenfrequency and always remains just above the lower edge of the continuum gap. The frequency decrease reflects the opening of the gap as the Shafranov shift increases. Its coupling from the antenna remains quite small and roughly constant. The mode 'b', on the other hand, is very sensitive to variations in the plasma equilibrium. Its frequency decreases strongly with increasing β_{pol}, by a factor 2 for $\beta_{pol} \simeq 2.4$. For $\beta_{pol} \simeq 2.25$ the two modes cross each other and for still higher β_{pol} mode 'b' enters the Alfvén continuum. The antenna coupling of mode 'b'

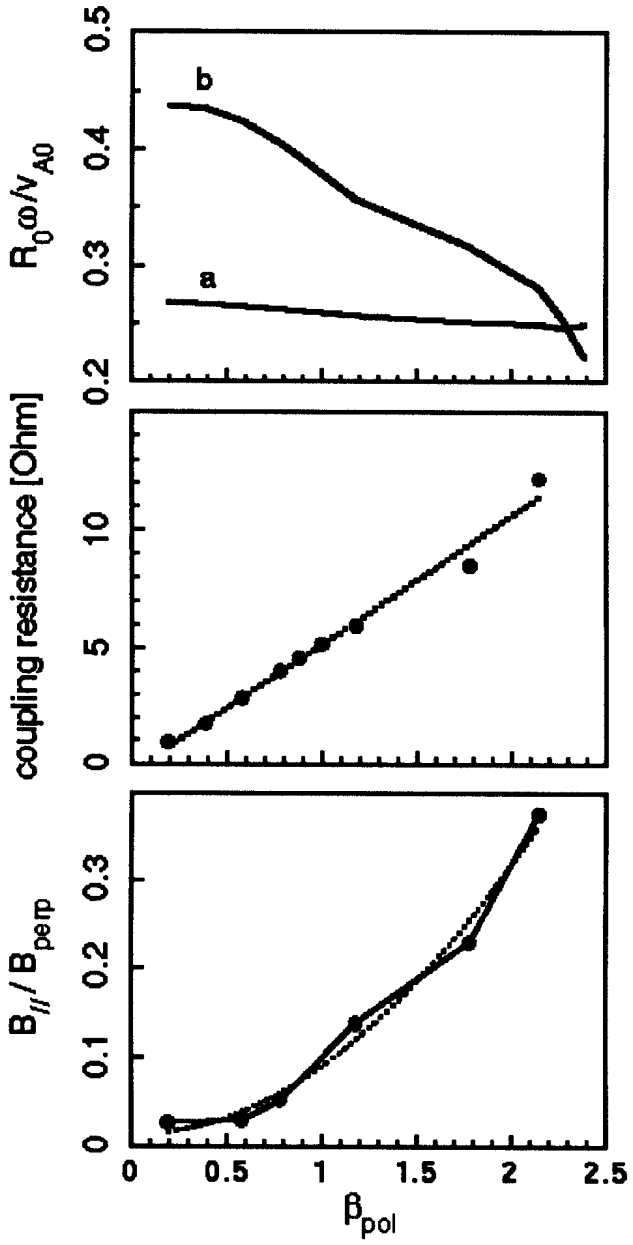

Figure 9: *Eigenfrequencies of the $n = 1$ TAEs 'a' and 'b' (top), JET saddle coils resistive coupling of mode 'b' (middle) and compressibility (ratio of amplitudes $B_{||}/B_{\perp}$)(bottom) of mode 'b' versus β_{pol} for the same parameters as in Fig.6 except the $p'(\psi)$ profile which is scaled by a constant factor.*

exhibits a remarkable behaviour: it is linearily proportional to β_{pol} (see Fig.9, middle). The compressibility of the mode (finite $B_{||}$) increases with β_{pol} (see Fig.9, bottom). The mode 'b' becomes less torsional: the ratio of amplitudes $E_n/E_\perp$ decreases from 15.4 for $\beta_{pol} = 0.78$ to 4.1 for $\beta_{pol} = 2.14$. Therefore gap modes are 'shear' Alfvén modes only in a loosely speaking sense. A practical consequence is that it may be hard to see the mode 'b' for low β_{pol} values in the antenna excitation experiments. We note also that the frequency decrease with increasing beta has been seen in the DIII-D experiment [34]. The factor 2 decrease that we found is of the same order as that reported in Ref. [34]. The authors of Ref. [34] have given another interpretation to this effect and named the high-beta TAE modes 'Beta-Induced Alfvén Eigenmodes' (BAE).

It should be noted that the external TAEs are really global: their wavefield is not localized near a particular gap position $q = (|m| + 1/2)/|n|$. Comparing Figs 7'b' with Fig.8, we conclude that there is no increase in mode localization with increasing n.

6 Stability of Alfvén eigenmodes

In the frame of the DKE model developped in Section 4.2 the stability of Alfvén eigenmodes (AE) is determined by a balance between the wave-particle power transfers to electrons, bulk and fast ions. Let us first analyze the parametric dependence of these powers for the cases of AEs.

The power transfer to bulk species depends on the ratios $\omega/|k_{||}|v_{the}$, $\omega/|k_{||}|v_{thi}$ and ω/ω_{ci} (see Eqs.(25)-(27)). The AE eigenfrequencies ω scale proportionally to the Alfvén velocity on axis v_{A0}, so the ratio $\omega/|k_{||}|v_{the}$ is proportional to $1/\sqrt{\beta_e}$, $\omega/|k_{||}|v_{thi}$ is proportional to $1/\sqrt{\beta_i}$, and $(\omega/\omega_{ci})^2$ is proportional to $1/n_0$. Thus for given $T_e(s)$, $T_i(s)$, $n(s)$ profile shapes the power to bulk ions and electrons for a given AE depends on β_e, β_i and on the bulk density n_0.

The DKE power to fast ions (Eqs.(28),(29)) depends on the ratio of the birth velocity v_0 to the parallel phase velocity v_p through the integrals I_0, I_1 and I_2 in Eqs.(28)(29). For a given AE, v_p scales proportionally to v_{A0}. The power to fast ions also depends on the fast ion pressure gradient, which can be measured by the fast ion density profile width $s_{1/2}$. The gradient term in Eq.(29) also contains a derivative of the electron temperature through the gradient of C (Eqs.(11)(12)). So the power to fast ions for a given AE, for a given T_e profile, depends on v_0/v_{A0}, $s_{1/2}$ and the fast ion density.

So one can characterize the overall global stability properties of a given AE mode in a plasma with given profile shapes of $T_i(s)$, $T_e(s)$ and $n_i(s)$ by the parameters β_e, β_i, β_f, v_0/v_{A0}, ω/ω_{ci} and $s_{1/2}$.

Of course the global overall stability of AEs depends also on the eigenmode wavefield

structure as we illustrate below.

In this section we analyze the stability of the lowest frequency TAEs that have no continuum damping. These modes are the most likely candidates for destabilization. The modes shown in Figs.7-8 are such TAEs. We use the perturbative approach, calculating the DKE powers (Section 4.2) with the wavefields obtained from the zero Larmor radius toroidal model (Section 4.1). (Remember, this approach does not hold when a KAW or SQEW is present. Continuum damping of low n modes was extensively studied in Ref [18] for a wide variety of shapes and profiles. High n continuum damping was analytically studied in Refs [35], [36]. Only for cases where the profile of $1/q\sqrt{\rho}$ is sufficiently peaked or hollow the continuum gaps do not overlap and all gap modes are continuum damped. Otherwise there may be TAEs 'threading' the gaps and thus exactly zero continuum damping. One cannot exclude such cases in a reactor since neither the density nor the q profile are easily controllable.)

6.1 TAE modes in JET in the presence of fusion alphas

Let us consider the $n = 1$ mode 'a' (Fig.7a) with the parameters $T_{e0} = 10keV$, $T_{i0} = 30keV$, in the presence of fusion alpha particles with density profiles defined by

$$n_f(s) = n_{f0}(1 - s^2)^{\kappa_f}, \tag{32}$$

and vary the profile peaking by varying κ_f. Moreover, we define the quantity $P(s)$ by the relation

$$P_{species} = \int_0^1 P(s)ds. \tag{33}$$

Fig.10 shows $P(s)$ of the different species, Eqs.(25)-(29), plotted versus s for $\kappa_f = 22$ which gives an alpha particle profile half-width $s_{1/2} = 0.176$. As expected, the destabilizing term P_f^{inhomo} peaks around $s = 0.15$ where the alpha particle density gradient is maximal. The fast particle stabilizing term P_f^{homo} shows a similar behaviour. The electron damping, on the other hand, is localized near $s = 0.8$ ($q = 1.5$) where eigenmode gradients are very large (see Fig.7a). The ion damping is maximal near $s \simeq 0.5$. This can be understood from the factor $\exp\{-(\omega/|k_{||}|v_{thi})^2\}$ in P^{homo}. Due to the $k_{||}$ variation with respect to s, the quantity $\omega/|k_{||}|v_{thi}$ is minimal near $s \simeq 0.5$. This example shows the importance of determining the overall stability globally. Local stability criteria would give instability if applied near $s = 0.2$ but stability if applied near $q = 1.5$ ($s = 0.8$). The influence of the eigenmode structure on the stability plays a crucial role. First, through the profile of eigenmode wave fields and their gradients (Fig.7). Second, through the profile of $k_{||}$.

Fig.10 shows that, in the presence of a TAE, alpha particles give their energy to the wave and the wave gives energy to bulk species. This opens thus the possibility of

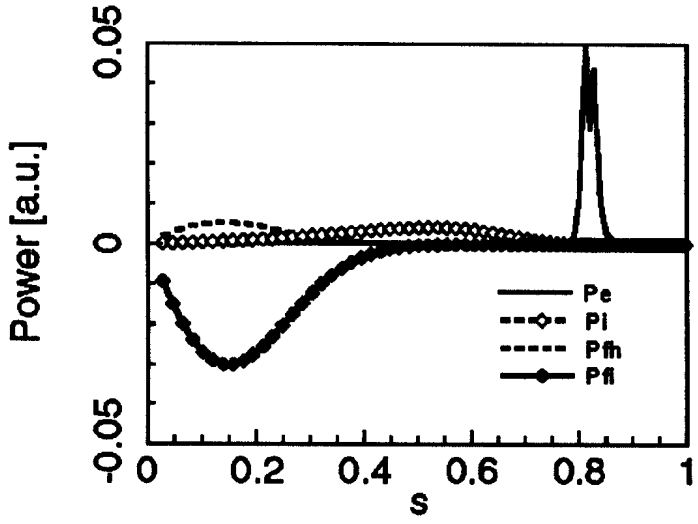

Figure 10: *Radial profiles of the wave-particle DKE power transfers to electrons (continuous line), bulk ions (open symbols) and alpha particles (dotted line: P_f^{homo}; filled symbols: P_f^{inhomo}) of the $n = 1$ internal TAE shown in Fig.7. JET parameters with $T_{e0} = 10keV$, $T_{i0} = 30keV$, fusion alpha particles with $n_f(s) = 10^{18}m^{-3}(1 - s^2)^{22}$, $s_{1/2} = 0.176$, $v_0/v_{A0} = 1.73$. The other parameters are the same as in Fig.6.*

fusion alpha power extraction by non-collisional processes. One can imagine a scenario in which a TAE would be excited by an antenna. If the TAE is stable but close to the marginal point, a large power transfer from alphas to bulk species can take place even with a moderate antenna power. Depending on plasma parameters, this power will be transfered preferentially to electrons or to bulk ions. For example, if we wish to maximize the power transfer to bulk ions, we should maximize the bulk ion Landau and TTMP dampings. This can be done by increasing the bulk ion temperature as we show below.

For the same parameters as in Fig.10 (except the fast particle density profile half-width $s_{1/2}$ and the central ion temperature T_{i0} which are varied) we show in Fig.11 the critical volume averaged alpha particle beta for marginal stability, $< \beta_f >_{cr}$, plotted versus the profile half-width $s_{1/2}$ for various central ion temperatures T_{i0}. The stabilizing effect of ion damping is clear for $T_{i0} \geq 20keV$. We note a remarkable behaviour of $< \beta_f >_{cr}$ vs $s_{1/2}$. For $s_{1/2} \lesssim 0.35$, flattening the fast particle profile is stabilizing as one can expect. But for $0.35 < s_{1/2} < 0.55$ flattening the fast particle profile actually destabilizes the mode: the reason is that an increasingly large fast particle pressure gradient is present near $s = 0.8$ ($q = 1.5$) where the eigenmode has a large amplitude (Fig.7a). This effect is not small : $< \beta_f >_{cr}$ is about a factor 2 larger for $s_{1/2} = 0.35$ than for $s_{1/2} = 0.55$. This means that about half of the fast particles would be lost if the fast particle profile widens beyond $s_{1/2} = 0.35$. For $s_{1/2} > 0.55$, flattening the fast

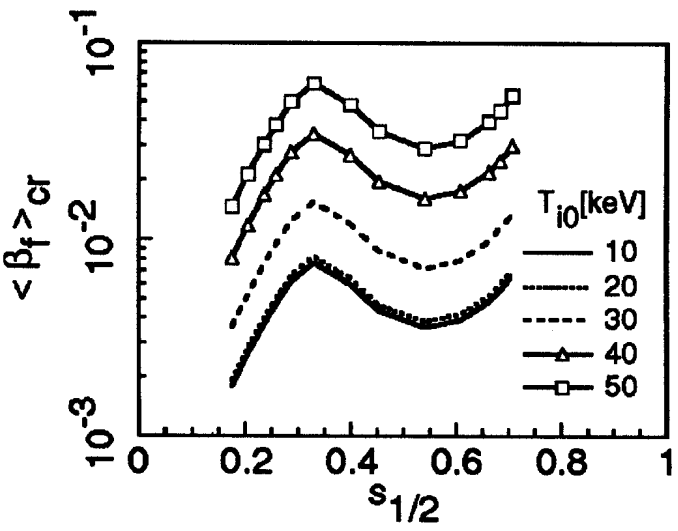

Figure 11: *Volume-averaged alpha particle beta for marginal stability, $< \beta_f >_{cr}$, of the $n = 1$ internal TAE shown in Fig.7a, versus alpha particle density profile half-width $s_{1/2}$, for various ion temperatures T_{i0}. The other parameters are the same as in Fig.6 (JET). (The mode is stable below the curves, unstable above).*

particle profile is again stabilizing because of the reduced fast particle pressure gradient.

6.2 TAE modes in DIII-D in the presence of NB-injected fast ions

In this section we consider the same sequence of plasma MHD equilibria as before but consider the case where both bulk ions and fast ions are deuterium species. Fast ions birth energy is $75keV$. The temperature and density profiles are chosen as $T_e(s) = T_{e0}(1-s^2)^{1/2}$, $T_i(s) = T_{i0}(1-s^2)^{1/2}$, $n(s) = n_0(1-0.9s^2)^{1/2}$ and $n_f(s) = n_{f0}(1-s^2)^{\kappa_f}$. We keep the ratio T_i/T_e constant at 1.25. Different values of bulk β, v_0/v_{A0} and ω/ω_{ci} are obtained by varying the bulk density n_0, temperatures T_{i0} and T_{e0} and magnetic field B_0 each over a wide range of values:

$$\begin{aligned} B_0 &= 0.6 - 2.25 \quad T \\ n_0 &= 1.3 - 30 \times 10^{19} \quad m^{-3} \\ T_{i0} &= 0.15 - 12.8 \quad keV \\ T_{e0} &= 0.12 - 10.3 \quad keV \end{aligned}$$

We set the major radius of magnetic axis at $1.8m$. These parameters overlap those of DIII-D TAE excitation experiments with NB injection [12], [13], [34].

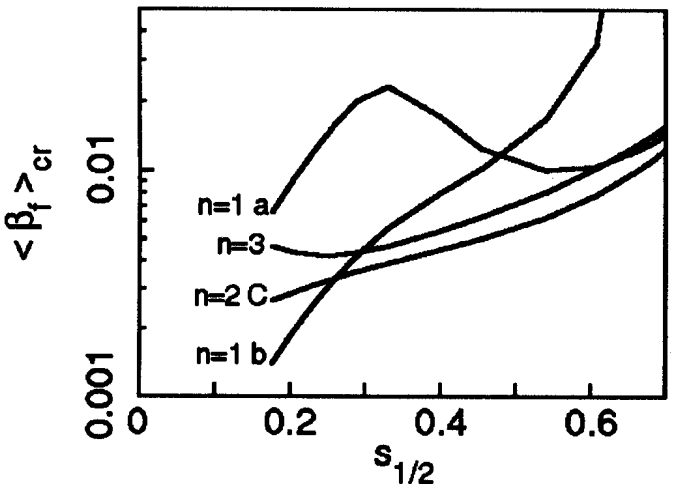

Figure 12: $< \beta_f >_{cr}$ *of the* $n = 1,2,3$ *TAEs shown in Figs.7-8 versus fast ion density profile half-width* $s_{1/2}$. *The parameters are typical of DIII-D:* $B_0 = 0.74T$, $\beta = 3.86\%$, $n_0 = 2 \times 10^{19} m^{-3}$, $T_{e0} = 2.05keV$, $T_{i0} = 2.56keV$, $v_0/v_{A0} = 1.048$.

Let us first study the fast particle critical beta corresponding to marginal stability, $< \beta_f >_{cr}$, for a range of fast ion profile widths $s_{1/2}$ obtained by varying the coefficient κ_f in Eq.(32). We show in Fig.12 $< \beta_f >_{cr}$ versus $s_{1/2}$ for the parameters $B_0 = 0.74T$, $n_0 = 2.0 \times 10^{19} m{-}3$, $T_{i0} = 2.56keV$, $T_{e0} = 2.05keV$. This gives a plasma bulk $\beta = 3.86\%$ and a ratio $v_0/v_{A0} = 1.048$. The $n = 1a$ internal TAE shows a similar behaviour as in Fig.11: the decrease in $< \beta_f >_{cr}$ between $s_{1/2} = 0.35$ and $s_{1/2} = 0.55$ is an effect of the particular eigenmode structure (Fig.7a). The $n = 1b$ external TAE does not show such a behaviour. The external mode amplitude (Fig.7b) is large near the magnetic axis and this gives a strong destabilization for peaked fast ion density profiles which is not balanced, as for the internal mode, by large electron damping (see Fig.10). For flat fast ion density profiles the internal mode is more unstable than the external mode because of the large mode amplitude and gradient of the internal mode near the $q = 1.5$ surface. The $n = 2$ and $n = 3$ external TAEs have stability limits very close to each other. This may explain why several n's are seen simultaneously in the experiment [13]. For small $s_{1/2}$, the $n = 3$ mode is more stable than the $n = 2$ mode, which is more stable than the $n = 1$ external mode. This can be understood from the smaller wave amplitude near magnetic axis for the $n = 3$ than for the $n = 2$ than for the $n = 1$ external mode.

We now study the TAE stability for various values of v_0/v_{A0}. The Alfvén velocity on axis, v_{A0}, is varied by changing the density n_0 and the temperatures T_{i0}, T_{e0} as $1/n_0$, keeping $B_0 = 0.74T$ constant, so that $\beta = 3.86\%$ is constant. Fig.13 shows $< \beta_f >_{cr}$ for

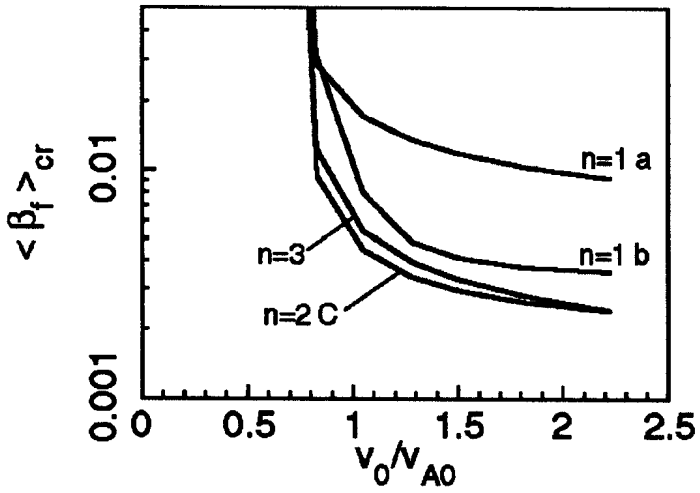

Figure 13: $< \beta_f >_{cr}$ *of the* $n = 1,2,3$ *TAEs shown in Figs.7-8 versus* v_0/v_{A0}, *for a fast ion density profile half-width* $s_{1/2} = 0.4$. *The parameters are* $B_0 = 0.74T$, $\beta = 3.86\%$. *The density* n_0 *is varied, the temperatures are varied as* $1/n_0$.

a fixed fast ion density profile width $s_{1/2} = 0.4$. For all TAEs, $< \beta_f >_{cr}$ is monotonically decreasing with v_0/v_{A0}. This is due to the increase in the number of resonant fast particles. Again, the similarity of the $n = 2$ and $n = 3$ stability limit is evidenced. We note also that TAEs can be destabilized for values of v_0/v_{A0} below unity: the reason is that the parallel phase velocity is smaller than v_A: $k_{||}$ is upshifted due to the toroidal coupling of several poloidal mode numbers m.

For the same plasma $\beta = 3.86\%$ and fast ion density profile width $s_{1/2} = 0.4$ we show in Fig.14 the TAE stability limits plotted versus B_0. The density n_0 is varied as B_0^2, and the temperatures are kept constant, so that β and v_{A0} are fixed. The circles correspond to $T_{i0} = 2.56keV$, $T_{e0} = 2.05keV$, which gives a fixed ratio $v_0/v_{A0} = 1.048$; the squares correspond to $T_{i0} = 1.25keV$, $T_{e0} = 1.0keV$, which gives a fixed ratio $v_0/v_{A0} = 1.5$. The magnetic field dependence is due mainly to two effects. First, the driving term, Eq.(29), is proportional to $\omega_{pf}^2/\omega_{cf}^3$, which is proportional to $1/B_0$ for this toroidal field scan since n_0 is varied as B_0^2; the damping terms, Eqs.(25)-(28), on the other hand, are proportional to ω_p^2/ω_c^2, which is constant for this toroidal field scan. Second, the damping due to $E_{||}$ contains a term proportional to ω/ω_{ci} which is proportional to $1/B_0$. (This term multiplies $\nabla \cdot \vec{E}$, so the damping due to $E_{||}$ is important when eigenmode gradients are large.) So increasing B_0 decreases both the drive and the damping, but in a different way. One can expect, for the $n = 1a$ internal TAE, that the stabilizing effect of decreasing B_0 is more important than for the $n = 1b$ external TAE, because it has larger eigenmode

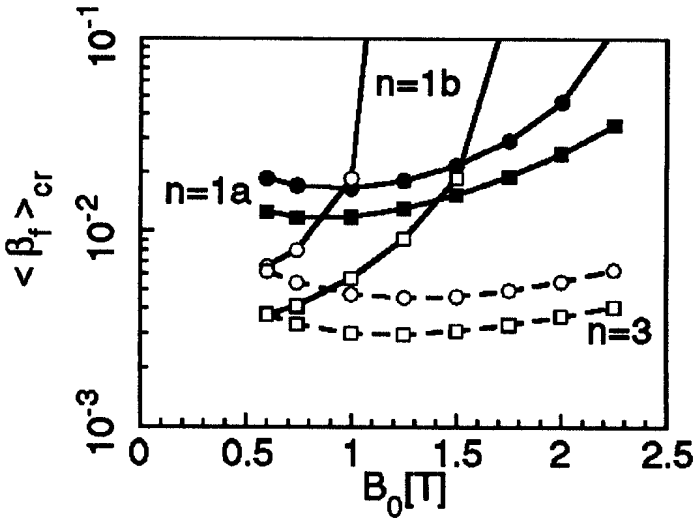

Figure 14: $< \beta_f >_{cr}$ *of the* $n = 1,2,3$ *TAEs shown in Figs.7-8 versus* B_0, *for a fast ion density profile half-width* $s_{1/2} = 0.4$. *The parameters are* $v_0/v_{A0} = 1.048$ *(circles),* $v_0/v_{A0} = 1.5$ *(squares),* $\beta = 3.86\%$. *The density is varied as* B_0^2.

gradients, so a larger $E_{||}$ damping (see Fig.10). Our results confirm this (Fig.14). The overall stabilization for low B_0 is also seen for the $n = 3$ TAE: it has larger eigenmode gradients than the $n = 1b$ external TAE (compare Fig.7 with Fig.8).

We now turn to the analysis of the β dependence of the TAE stability. We consider the $n = 1b$ external TAE and study the marginal stability $< \beta_f >_{cr}$ versus v_0/v_{A0} for different β values. The results are shown in Fig.15, for a given fast ion density profile width $s_{1/2} = 0.4$. The parameter v_0/v_{A0} is varied by changing the bulk density n_0 and a constant β scan is obtained by changing the bulk temperatures as $1/n_0$. For large v_0/v_{A0} the TAE is stabilized when β increases, due to enhanced electron and ion Landau damping. On the other hand, increasing β is destabilizing for small v_0/v_{A0}: the minimum v_0/v_{A0} for instability goes from 1 for $\beta = 1\%$ down to 0.7 for $\beta = 5.5\%$. Increasing β is lowering the eigenfrequency of this mode (see Fig.9). Consequently the parallel phase velocity is decreasing and more fast particles can destabilize the mode. Therefore the threshold in v_0/v_{A0} is going down with increasing beta for this mode.

We note that for $v_0/v_{A0} < 2$ and $\beta = 1\%$ we have $< \beta_f >_{cr} > 0.2\%$, which is larger than the estimated $< \beta_\alpha >$ in TFTR D-T experiments [37] in which no sign of TAE activity was reported.

More cases are analyzed in Ref.[38]. We have found that $< \beta_f >_{cr}$ is in almost all cases always larger than 0.1%. The only exceptions are extremely peaked fast ion density profiles ($s_{1/2} < 0.15$) for the $n = 1(b)$ external TAE. When compared with the DIII-D

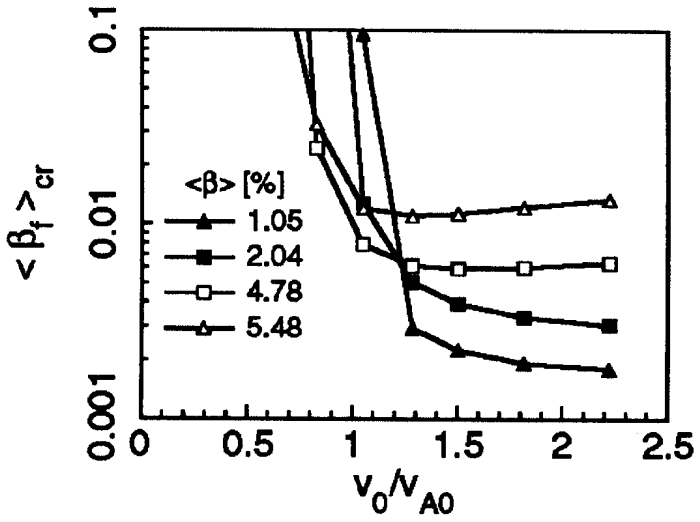

Figure 15: $< \beta_f >_{cr}$ *of the* $n = 1b$ *external TAE shown in Fig.7 versus* v_0/v_{A0}*, for a fast ion density profile half-width* $s_{1/2} = 0.4$, $B_0 = 0.74T$*, and various values of bulk* β*.*

experimental database [13], the minimal value of v_0/v_{A0} above which TAE instabilities are seen, the typical values of $< \beta_f >$ that can make TAEs unstable, the fact that several n's are simultaneoulsy destabilized, the fact that the $n = 1$ TAEs are most often more stable than higher n modes, the TAE eigenfrequencies, are well reproduced by our model. These encouraging results make us confident that our model can be applied for a reliable quantitative prediction of the TAE stability limit in a reactor. Another check of our model is to compare the perturbed magnetic field in the vacuum with the experimental probe measurements. For this, a case by case analysis is required including a careful equilibrium reconstruction. First results obtained with the PENN code on DIII-D shot 71524 at 1875ms indicate that the perturbed magnetic field B_θ has maximum amplitude at the outboard (low field side) of the torus. We have noted also that the poloidal structure of B_θ at the probe locations does not reflect simply the B_θ structure in the plasma near the edge.

Our model could be improved in the following ways. First, for cases where the interaction with kinetic waves is important, e.g. when a TAE is intersecting the continuum, we can go beyond the perturbative approach with the global toroidal FLR model developped in Section 4.3. Second, other kinetic effects could be included in the wave-particle transfer, such as the finite orbit width or the effect of trapped particles.

We have shown that in any case a global approach must be used in order to obtain a reliable quantitative prediction. There are two reasons for that. First, the fast ion

drive, damping on electrons, damping on bulk ions and damping on fast ions take place at different radial positions. Second, the TAE wave fields extend over the whole plasma cross-section. There is no mode localization, even with increasing n. This fact complicates the analysis of experiments in which there is a toroidal velocity shear. The effect of the velocity shear is then not simply a Doppler shift of the eigenfrequencies. There may be additional effects on the mode structure and therefore on the damping and drive.

7 Conclusions

We have shown how progresses have been made in the theoretical understanding of Alfvén waves in fusion plasmas. With the advent of more and more performing numerical tools and computers, we have been able to study realistic geometries with increased accuracy and with more and more physical effects included in the models.

Roughly speaking, the theory has been able to make correct predictions first on the real part of the frequencies of the Alfvén spectrum, and then on the imaginary part (damping - growth rates) as well. The effect of Alfvén waves on particle and energy confinement has been observed to be important. The theory is in the present stage not really able to predict this behaviour, partly because the anomalous transport is anyway not really understood. Non-linear kinetic theories are required, and this would imply solving a 3D configuration space and at least 2D velocity space time evolution problem.

Acknowledgments

This work was partly supported by the Swiss National Science Foundation. We thank Dr. K. Appert for his support, Dr. H. Lütjens for the equilibrium code CHEASE and Drs A. D. Turnbull, W. W. Heidbrink and M. Vukovic for interesting discussions.

References

[1] DE CHAMBRIER, A., COLLINS, G.A., DUPERREX, P.A., et al., Proc. 4th Int. Symposium Heating in Toroidal Plasmas (Int. School of Plasma Physics, Varenna, 1984), Vol.I, p.153.

[2] COLLINS, G.A., HOFMANN, F., JOYE, B., et al., Phys. Fluids **29** (1986) 2260.

[3] APPERT, K., COLLINS, G.A., HOFMANN, F., et al., Phys. Rev. Lett. **54** (1985) 1671.

[4] EVANS, T.E., VALANJU, P.M., BENESH, J.F., et al., Phys. Rev. Lett. **54** (1984) 1743.

[5] HERSHKOVITZ, N., MOROZ, P., PROBERT, P., et al., to appear in Proc 15th IAEA Int. Conf., on Plasma Phys. Control. Nucl. Fusion Research, Seville, Spain (1994).

[6] FU, G.Y., VAN DAM, J.W., Phys.Fluids B **1** (1989) 1949.

[7] CHENG, C.Z., Phys.Fluids B **3** (1991) 2463.

[8] BELIKOV, V.S., KOLESNICHENKO, YA.I., SILIVRA, D.A., Nucl.Fusion **32** (1992) 1399.

[9] BIGLARI, H., ZONCA, F., CHEN, L., Phys.Fluids B **4** (1992) 2385.

[10] FU, G.Y., CHENG, C.Z., WONG, K.L., Phys.Fluids B **5** (1993) 4040.

[11] WONG, K.L., FONCK, R.J., PAUL, S.F., ET AL., Phys.Rev.Lett. **66** (1991) 1874.

[12] HEIDBRINK, W.W., STRAIT, E.J., DOYLE, E., ET AL., Nucl.Fusion **31** (1991) 1635.

[13] STRAIT, E.J., HEIDBRINK, W.W., TURNBULL, A.D., CHU, M.S., DUONG, H.H., Nucl.Fusion **33** (1993) 1849.

[14] VACLAVIK, J., APPERT, K., Nucl. Fusion **31** (1991) 1945.

[15] ROSENBLUTH, M.N., RUTHERFORD, P.H., Phys. Rev. Lett. **34** (1975) 1428.

[16] CHENG, C.Z., CHANCE, M.S., Phys.Fluids **29** (1986) 3695.

[17] BETTI, R., FREIDBERG, J.P., Phys. Fluids B **3** (1991) 1865.

[18] VILLARD, L., FU, G.Y., Nucl.Fusion **32** (1992) 1695.

[19] METT, R.R., MAHAJAN, S.M., Phys.Fluids B **4** (1992) 2885.

[20] APPERT, K., VACLAVIK, J., VILLARD, L., Phys. Fluids **27** (1984) 432.

[21] APPERT, K., GRUBER, R., TROYON, F., VACLAVIK, J., in Heating in Toroidal Plasmas (Proc. 3rd Joint Varenna-Grenoble Int. Symp. Grenoble, 1982), Vol.1, CEC, Brussels (1982) 203.

[22] APPERT, K., HELLSTEN, T., LÜTJENS, H., SAUTER, O., VACLAVIK, J., VILLARD, L., in Plasma Physics (Proc. 7th Int.Conf.Kiev, 1987), Invited papers, Vol.2, World Scientific, Singapore (1987) 1230.

[23] APPERT, K., HELLSTEN, T., VACLAVIK, J., VILLARD, L., Plasma Phys. Control. Fusion **30** (1988) 1195.

[24] SAUTER, O., VACLAVIK, J., accepted for publication in Comput. Phys. Commun. (1994); Lausanne Report LRP 495/94 (1994).

[25] LÜTJENS, H., BONDESON, A., ROY, A., Comput.Phys.Commun. **69** (1992) 287.

[26] VILLARD, L., APPERT, K., GRUBER, R., VACLAVIK, J., Comput.Phys.Rep. **4** (1986) 95.

[27] KOCH, R., Phys.Lett. A **157**, (1991) 399.

[28] SHAFRANOV, V.D., in Reviews of Plasma Physics, edited by M.A.Leontovich (Consultants Bureau, New York, 1967) Vol.3.

[29] BRUNNER, S., VACLAVIK, J., On Absorption of Low Frequency Electromagnetic Fields, Lausanne Report LRP 471/93 (1993); to appear in Theory of Fusion Plasmas (Proc. Joint Varenna-Lausanne Int. Workshop, Varenna, 1994), Editrice Compositori, Bologna, Italy.

[30] BRUNNER, S., VACLAVIK, J., Phys. Fluids B **5** (1993) 1695.

[31] BATCHELOR, D.B., JAEGER, E.F., WEITZENER, H., in Theory of Fusion Plasmas (Proc. Joint Varenna-Lausanne Int. Workshop, Chexbres, 1988), Editrice Compositori, Bologna, Italy.

[32] JAUN, A., APPERT, K., LÜTJENS, H., VACLAVIK, J., VILLARD, L., to appear in Theory of Fusion Plasmas (Proc. Joint Varenna-Lausanne Int. Workshop, Varenna, 1994), Editrice Compositori, Bologna, Italy.

[33] POEDTS, S., KERNER, W., GOEDBLOED, J.P., KEEGAN, B., HUYSMANS, G.T.A., SHWARTZ, E., Plasma Phys.Control.Fusion **34** (1992) 1397.

[34] HEIDBRINK, W.W.,STRAIT, E.J., CHU, M.S., TURNBULL, A.D., Phys. Rev. Lett. **71** (1993) 855.

[35] ROSENBLUTH, M.N., BERK, H.L., VAN DAM, J.W., LINDBERG, D.M., Phys. Rev. Lett. **68** (1992) 596.

[36] ZONCA, F., CHEN, L., Phys.Rev.Lett. **68** (1992) 592.

[37] STRACHAN, J.D., ADLER, H., ALLING, P., ET AL., Phys.Rev.Lett. **72** (1994) 3526.

[38] VILLARD, L., BRUNNER, S., VACLAVIK, J., submitted for publication to Nucl. Fusion (1994); Lausanne Report LRP 500/94.